2022 18th International Conference on Distributed Computing in Sensor Systems (DCOSS) | 978-1-6654-9512-7/22/$31.00 ©2022 IEEE | DOI: 10.1109/DCOSS54816.2022.00064

Multi-physics Analysis of Electromagnetic Wave Propagation and Photothermal Heating in Human Tissues at Terahertz and Optical Frequencies

Innem V.A.K Reddy
Department of Electrical Engineering
University at Buffalo
NY, USA
innemven@buffalo.edu

Josep M. Jornet
Department of Electrical and Computer Engineering
Northeastern University
Boston, MA
j.jornet@northeastern.edu

***Abstract*—We present a custom-built, multi-physics model to investigate electromagnetic wave propagation in extreme random media such as human tissue and study its subsequent photothermal effects. The proposed finite-element model consists of two segments – the first one estimates the intensity distribution along the beam path, while the second calculates the increase in temperature due to the wave distribution inside the tissue. We determine the intensity variation in the tissue using the radiative transfer equation and compare the results with Monte Carlo analysis and existing analytical models. The intensity information is then utilized to predict the rise in temperature with a bioheat transfer module, powered by Pennes' bioheat equation. The model is parametric, and we perform a systematic photothermal analysis to recognize the crucial variables responsible for the temperature growth inside the tissue, particularly for terahertz and near infrared optical frequencies. Our numerical model can serve as a benchmark for intrabody communication studies involving complex heterogeneous media.**

***Index Terms*—Electromagnetic wave propagation, Radiative transfer equation, Photothermal effects, Pennes' bioheat equation**

I. Introduction

In recent years, there has been a spike in the interest for intrabody communications (IBC) [1], [2], as it is vital for wearable sensors [3] or implants [4] in a human body. The advancements in nanobiosensing systems have facilitated new modalities to monitor the health of an individual or even detect diseases [3] in the early stage. Such intelligent nanosensing networks work in-vivo, usually embedded in the human tissue. These complex systems often require a wireless communication link to exchange information. Different communication technologies have been considered for IBC, including molecular signals [5], acoustic signals [6], electric and magnetic currents [7], and electromagnetic (EM) waves. Focusing on the latter, originally, researchers used IBC with the human body as a waveguide while treating the tissue as a communication channel, and relied mostly on low-frequency EM. At present, the miniaturization of sensors has shifted the paradigm of communications from low-frequency EM waves (microwaves) to high-frequency EM waves (terahertz band and beyond), paving the way to nanosensor networks [8], [9]. Such high-frequency operable nanonetworks typically use advanced nanophotonic and nanoelectronic sensors and require a new approach to realize effective communication schemes. This demand led to the realization of a new branch called - the Internet of Nano-Things [10] and Nano-Bio-Things [11].

Compact nanobiosensors [12] are typically designed to stay in contact with the sensing medium such as blood and are embedded inside human tissue. The tissue is a complicated heterogeneous system with multiple layers. It poses a significant challenge [13] as EM waves experience variable absorption through layers. Also, high-frequency EM waves contain significantly smaller wavelengths than the surrounding tissue and can experience scattering. Overall, such a system results in a complicated communication channel and restricts the placement of the sensor inside the tissue. Although one could mitigate this issue by using a high power source, it could result in other consequences such as photothermal effects [14]–[16]. Over the past years, there have been extensive studies on channel modeling at the nanoscale [17] along with the photothermal effects. The works utilized models at the cellular level and extended the studies from terahertz frequencies to optical frequencies [18], [19]. We believe it is essential to extend these studies to large-scale modeling that involves human tissues and comprehend a safe way of utilizing EM waves for IBC.

Electromagnetic wave interaction with human skin is an intriguing subject that excited researchers in the past and led to several mathematical models [20] to estimate the propagation inside the tissue. Some of the notable ones include Monte Carlo analysis [21], Diffusion approximation of the radiative transfer equation [22] or K-M theory [23], to name a few. Of these approximations, Monte Carlo analysis is regarded as the most accurate [20] as it estimates propagation by considering each photon as a ray of light and tracks its path in the tissue. However, it is computationally expensive and requires substantial computational resources and time. The next best approach is the diffusion approximation [20]. This method uses partial differential equations to calculate the intensity variation and requires less time.

In this paper, we use the abovementioned approaches to estimate the EM wave distribution inside tissue and couple

2325-2944/22/$31.00 ©2022 IEEE
DOI 10.1109/DCOSS54816.2022.00064

the data to a heat transfer module. In the past, to estimate the heat distribution inside the tissue, some groups used Fourier heat conduction [24], hyperbolic heat conduction [25], thermal wave model of bioheat transfer [26], and dual-phase lag model [27]. All these models work accurately and are specifically tuned to work adequately for heterogeneous media by considering the microscale thermal variations [28]. However, in our case, we deal with macroscale variation of heat transfer, and hence we employ Pennes' approximation [29] of the bioheat equation (PBE) to calculate the heat distribution. Also, the equation incorporates heat from blood perfusion and metabolism, resulting in a practical scenario [30].

Our model combines the diffusion approximation of the radiative transfer equation and Pennes' bioheat equation to calculate the intensity distribution inside the tissue along with the temperature rise. Such combined models are highly beneficial not only for investigating IBC but also for studies like photodynamic therapy [31], photothermal therapy [32], photoacoustic imaging and spectroscopy [33], [34], and optical coherence tomography [35], among others, as one could calculate the intensity distribution and photothermal effects in one go. We illustrate the multi-physics model as a standard to perform complex channel modeling on large-scale domains such as human tissue and predict the photothermal effects accurately in less time.

The remainder of the paper is organized as follows. In Sec. II, we introduce the computational model with the physics modules used to estimate the tissue's intensity distribution and temperature rise. In Sec. III, we present the results in a step-by-step manner. First, we discuss wave propagation in the tissue by employing different wavelength sources and discuss the significance of modeling by utilizing different tissue properties. We then present the photothermal analysis by varying the source's power and beam waist to showcase the temperature variation. We also showcase a technique to control the temperature rise by modulating the power of the incident EM source. We finally conclude the work in Sec. IV.

II. Computational Model

We use COMSOL [36], a finite element analysis (FEM) software, to build the theoretical model. We built a 2D axially-symmetric tissue geometry composed of three layers, epidermis, dermis, and blood-infused fat. These three layers imitate the topmost portion of human tissue. Since it is a parametric model, one can easily vary the tissue's thickness, absorption, and scattering coefficients. The layers are surrounded by an infinite element domain, mimicking a semi-infinite region. We utilized two physics modules; one takes care of the intensity distribution while the other assists in determining the temperature rise.

To estimate the intensity distribution, we built a custom module that utilizes diffusion approximation of the radiative transfer equation [37], which is given by:

$$\left(\frac{1}{v}\frac{\partial}{\partial t} - D\nabla^2 + \mu_a\right)\Phi(\overrightarrow{r},t) = q_0(\overrightarrow{r},t) \qquad (1)$$

where v is the speed of wave, which is speed of light in this case, D is the diffusion coefficient given by $D = \frac{1}{3(\mu_a+\mu_s{}')}$, μ_a is the absorption coefficient, $\mu_s{}'$ is the reduced scattering coefficient, $\Phi(\overrightarrow{r},t)$ is the fluence rate and $q_0(\overrightarrow{r},t)$ is the source. Here, we use the fluence rate in the place of Irradiance. Irradiance is the radiation power incident on the flat surface, while the fluence rate accounts for the power incident on a sphere of a unit cross-section. Considering the absorption and scattering inside the tissue, the fluence rate seems more appropriate in our case. Generally, each layer in the tissue will have a different set of absorption and scattering coefficients. Consequently, the diffusion varies in each layer. On top of that, the absorption and scattering coefficients depend on the incident beam's wavelength and intrinsic tissue properties such as melanin content. Hence, diffusion can vary from person to person depending on the incident wavelength. So, it is critical to have a parametric model that accounts for all the variations. We built our model, keeping this aspect in mind, and made it parametric.

We use the Dirichlet boundary condition at the incidence boundary. There is also a provision to define the incident beam shape along with the power, and beam waist, as per requirements. In this paper, we used a Gaussian beam as it is the most common beam profile. One of the limitations of the diffusion approximation is that it does not incorporate the information on the refractive index of the tissue layers. Hence, the model does not calculate the reflections at the incidence and between the layers. It estimates the intensity distribution of the incident wave by assuming a uniform refractive index. Hence, for the given model, it is crucial to validate the intensity distribution study before heading to the photothermal analysis. To validate the numerical model, we compared the results with an analytical system that utilizes Beer-Lambert's law and a Monte Carlo simulation (MC) developed by Steven Jacques and his group [38], [39]. The analytical system is a 1D model and considers both absorption and scattering in the tissue as absorption. Coming to the MC model, it utilizes a 2D domain and accounts for absorption, scattering as well as the refractive index of individual layers. It assumes Electromagnetic (EM) waves as several rays, and each ray is given a certain weight at the incidence. As the ray propagates, depending on the absorption and scattering coefficients of the layer, the weight decreases, and the direction of the ray changes. The model plots millions of such rays and determines the intensity distribution inside a tissue. As it incorporates all the intricacies in light-tissue interaction, the model is considered the closest to reality. However, it is time-consuming and requires substantial computational resources. Our model, on the other hand, can estimate the wave propagation in 3D and solve the problem in less time, while generating results close to that of the MC approach. We present the comparison of these models in the next section.

Once the model calculates the intensity distribution inside the tissue using the diffusion approximation of radiative transfer equation, it feeds the data to the heat transfer analysis

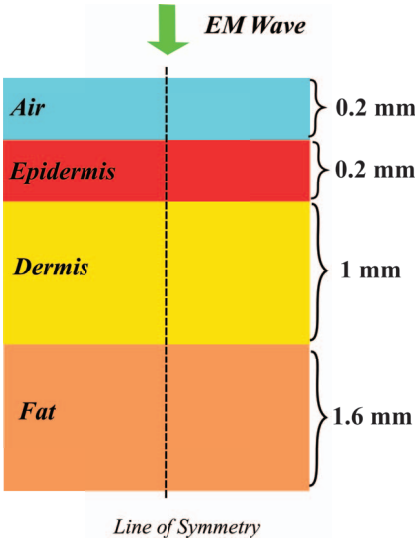

Fig. 1. Computational domain comprising of Air, Epidermis, Dermis and blood-infused fat. EM wave is incident on the air domain and propagates through tissue layers. The line of symmetry for simulation is indicated in the above figure.

module. This module utilizes Pennes' bioheat equation (PBE) to calculate the temperature distribution inside the tissue. The equations are given by:

$$\rho C_p \frac{\partial T}{\partial t} + \rho C_p u.\nabla T + \nabla.q = Q + Q_{bio} \tag{2}$$

$$Q_{bio} = \rho_b C_{p,b} \omega_b (T_b - T) + Q_{met} \tag{3}$$

where, ρ is the tissue density, C_p is the specific heat capacity of the tissue, T is the local tissue temperature, q is the boundary heat flux, Q is the source, Q_{bio} is the bioheat source, which is a combination of metabolic heat given by Q_{met} and blood perfusion related heat source, ρ_b is the density of blood, $C_{p,b}$ is the specific heat capacity of blood, ω_b is the blood perfusion rate and T_b is the blood temperature .

The intensity observed inside the tissue layers acts as the heat source, increasing the tissue's temperature. However, the bioheat source Q_{bio} acts as negative feedback and aids in reducing the temperature. Our human body continuously regulates the temperature and maintains it at a standard temperature ($37°C$). It uses the blood under the tissue as a medium to transport heat and maintain body temperature. For example, if we touch a cold surface, the temperature drops down at the tissue's surface. Eventually, the body restores the temperature to the previous value by continuously transferring the heat with blood flow. Similarly, when an EM wave with sufficiently high power is incident on a surface, there is feedback from the body that works to bring down the temperature to the standard value. We supply this feedback in the form of Q_{bio}. Heat transfer can also occur externally through airflow (convection) around the skin. We considered this effect and applied a heat flux (q) boundary condition to the top layer of the tissue. This heat flux also assists in reducing the temperature. However, it depends on the heat transfer coefficient and external temperature. If the surrounding temperature is low and the heat transfer coefficient is high, the tissue temperature reduces fast. We use this equation along with the boundary conditions mentioned above to analyze the temperature distribution inside human tissue.

Since the equations are time-dependent, we can assess the temperature variation in time. When an EM wave is incident on a tissue for a period of time, due to the negative feedback of heat source from the body, the temperature rise is predicted to take an asymptotic shape. Although there is a continuous input from the EM source, the negative feedback from the metabolic heat and the heat flux brings down the value. These parameters are strictly dependent on the surroundings and body conditions. Hence, the regulated temperature value is subject to change. Figure 1 shows the 2D-axisymmetric model with the line of symmetry representing the center of the tissue layers. We built a 2D-axisymmetric model as the computational domain is azimuthally symmetric. It yields distribution in 3D with solving time of the 2D model. As per the geometry, as mentioned before, the tissue geometry has three layers while the computational domain consists of four layers - Air, Epidermis, Dermis, and Blood-infused fat. This configuration is the most common human tissue model. Coming to the thickness of layers, we chose 0.2mm for air layer, 0.2mm for the epidermis, 1mm for the dermis layers, and 1.6mm for the blood-infused fat. As the fat layer consists of several blood vessels and capillaries, we consider the whole system as blood-infused fat. The EM wave is incident on the top layer as shown by the arrow, and one can define the beam profile and the beam waist. Using this model, we collect 1D and 2D plots to estimate the intensity distribution and the tissue's temperature rise.

III. Results and Discussion

This section presents the theoretical analysis of EM wave propagation and the corresponding photothermal effects inside the tissue. EM wave spectrum consists of several bands ranging from radio waves with extremely long wavelengths to gamma rays with extremely short wavelengths. Present-day advanced nanophotonic chips or wearable devices, that are typically used for intra-body communications work at non-ionizing high-frequency bands, leaving us with visible, infrared, and microwave bands. We chose near-infrared (NIR) and terahertz (THz) bands for our simulations. Human tissue experiences high scattering in the NIR range and high absorption in the THz range, and we believe these two bands signify and represent the overall behavior of EM spectrum. As discussed before, our custom-built module performs the wave propagation and passes the intensity information to the next module, i.e., the heat transfer module. From this module, we get the results related to the increase in temperature and its distribution inside the tissue. Here, we present these results systematically, along with the parametric analysis. This study gives a better idea of the specific parameters reasonable for wave propagation and temperature regulation.

A. Wave Propagation - NIR regime

The NIR regime in the EM spectrum is considered a biological window as it offers higher penetration depths due to the high scattering coefficient of tissue layers. Here, we chose a source of 1030nm wavelength to illustrate the wave propagation. As mentioned in the previous section, we tested two other techniques (analytical and MC model) along with the diffusion approximation (DA) for reference. For this analysis, we collected and used the absorption and scattering coefficients of the individual tissue layers [40]. The thickness is the same, as shown in Figure 1. We chose an arbitrary power along with a beam waist of 0.2mm. Figure 2 below summarizes the distribution observed for MC analysis, diffusion approximation, and the 1D plot through the center. Since the initial layer is composed of air with zero absorption and scattering, the incident wave passes through the layer without reducing the intensity. The same can be observed in Figure 2(a) and (b). While coming to the tissue layers, the distribution varies drastically. This change is due to the high scattering coefficient observed in the tissue layers. MC analysis considers individual rays, and hence their scattering leads to a change in the direction of rays that results in a non-uniform distribution. This approach is more practical as it is close to the real-world scenario. On the other hand, the FEM model utilizes a diffusion approximation that does not incorporate ray scattering, literally. It uses the scattering coefficient in the diffusivity parameter, and the inclusion is typically to generate an approximate intensity variation. In the MC analysis, there is a focus at the end of the epidermis layer, which results from high scattering. However, in the DA analysis, the distribution is uniform along the wave propagation path. Apart from the lateral direction variations, both the techniques agree on the intensity distribution accurately. The same can be observed from the 1D plots, as shown in Figure 2c. We normalized the intensity for a better understanding. The MC analysis plot has a peak, signifying the presence of a focus. This focus is close to 0.4mm, i.e., at the end of the epidermis. After that, there is a substantial drop in the intensity along the path and reaches close to zero by 3mm. On the other hand, the DA plot follows a similar trend as the MC plot. It drops to zero by 3mm, but at a slightly different rate. Finally, the modified analytical model, which is based on Beer-Lambert law, predicts the trend with high accuracy. This type of analytical model offers a quick, accurate solution but is restricted to a 1D analysis.

B. Wave Propagation - THz regime

In this section, we perform a similar analysis as before but with a THz wave. THz regime acts as a bridge between IR and microwave bands. In this regime, the wavelengths vary between 30 μm and 3 mm. The wavelengths are comparable to the domain, so the scattering is no longer an essential parameter for this analysis. Water has high absorption peaks in the THz regime, and as the human body is composed of 70% water, human tissue will experience high absorption [41], [42]. We observe similar behavior in Figure 3, where the wave hardly enters the dermis layer. The distributions, Figures 3a and 3b are identical as they can be considered pure-absorption models. The 1D plots also agree well and can be noticed in Figure 3c.

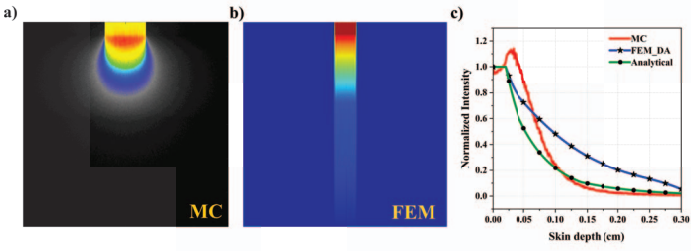

Fig. 2. Comparison of wave propagation with three different techniques; (a) 2D plot showcasing the distribution predicted with MC analysis, (b) 2D plot showcasing the distribution predicted with diffusion approximation using FEM software, COMSOL, (c) 1D plot signifying the normalized intensity variation observed along the line of symmetry.

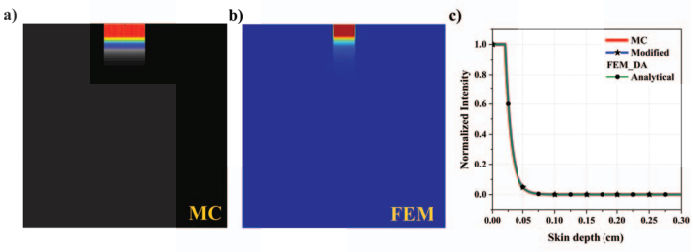

Fig. 3. Comparison of wave propagation in the THz regime (a) 2D plot showcasing the distribution predicted with MC analysis, (b) 2D plot showcasing the distribution predicted with diffusion approximation using FEM software, COMSOL, (c) 1D plot signifying the normalized intensity variation observed along the line of symmetry.

C. Melanin content - effects

This section demonstrates the effect of melanin content [43] variation over the intensity distribution in the skin. It is a well-known fact that melanin content in the skin plays a vital role in light absorption. The melanin content and absorption directly correlate; the higher the melanin concentration, the greater the absorption. In general, light-skinned individuals possess less melanin content when compared to dark-skinned individuals. This variation affects the intensity distribution substantially. To illustrate the same, we chose a visible-light wavelength of 694nm. It is the wavelength of the most commonly used light sources readily available. Figure 4(a) compares the distribution predicted by three methods - MC analysis, FEM-DA analysis, and an analytical model. This plot is similar to Figure 2, except that the intensity drops down reasonably quickly. Since the absorption and scattering coefficients are higher than the NIR region, this behavior seems valid. Once we determined that the FEM-DA approach generates similar MC and analytical results, we varied the melanin content parameter. This parameter is not fixed and is wavelength-dependent. We categorized the data into three sections, depending on the melanin fraction in individuals. The plot Figure 4(b) summarizes the intensity distribution, and one can notice a distinct variation for all

three sets of individuals. This plot showcases the challenge of designing a communication channel that could work for all individuals. When we choose EM wave as a mode of communication for bio-sensors or implants, these intensity plots will help determine the device's placement based on the melanin content.

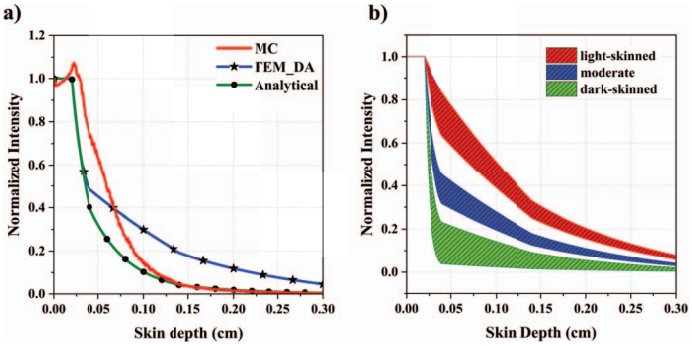

Fig. 4. (a)1D intensity plot with all three analysis - MC, FEM-DA and analytical model. The analysis is performed at 694nm wavelength, (b) FEM-DA analysis by varying the melanin content inside the tissue.

D. Photothermal analysis

In this section, we will discuss the photothermal effects associated with the EM wave interaction with human skin. As discussed before, EM waves carry a broad spectrum range, and depending on the frequency or wavelength of the incident light, human skin can behave differently. For example, high-energy EM waves such as UV could cause skin cancer. One can notice this particular behavior in light-skinned individuals, as the light is absorbed less, again due to the low melanin content. When it comes to the low energy/low-frequency EM waves, especially Radio waves and microwaves, that are frequently used for communication, they do not pose any risk, irrespective of the melanin content. Nevertheless, if the power is substantially high, the energy absorbed is dissipated as heat, increasing the tissue's temperature. However, it is challenging to establish high coherence energy sources, especially in the radio and microwave regions. The only part of the spectrum with readily available high energy sources is visible and IR. The invention of the laser and the abundant applications in this spectrum region boosted the research leading to a sturdy increase in sources ranging all over the spectrum. In the following sections, we will showcase the photothermal effects associated with NIR and THz sources.

E. Varying the power and beam waist of the source

Here, we performed parametric analysis by varying the power and beam waist of the sources. The beam, here, is incident normal to the surface, as shown in Figure 1. We divided the tissue into two parts - skin and fat. Skin is composed of epidermis and dermis layers. The model assumes a continuous blood flow in these regions, and blood acts as the medium of heat transport between regions. We also applied a heat flux boundary at the top of the skin, as there will be heat transfer at the interface due to the airflow (convection) outside the body. For analysis, we chose the wavelengths - 1200nm and 300 μm. We chose these wavelengths as one of them leads to a scattering dominant distribution, while the other to an absorption dominant behavior. The NIR wavelength 1200nm has a high scattering coefficient, while the far-IR or THz wavelength 300 μm is the opposite in nature, with high absorption and low scattering coefficient. As a first step, we fixed the beam waist to 1mm and varied the incident source's power. We chose a different range of powers for these wavelengths based on the present-day availability of sources. In the NIR beam case, the power is varied from 10mW to 250mW, while for the THz beam, the power is varied from 0.5mW to 5mW. Figure 5 represents the rise in temperature observed in both these cases. The data represents the maximum temperature observed in the skin. As explained in the introduction section, the human body continuously puts effort to stabilize the temperature change imparted by an external source. We observe an asymptotic curve due to this feedback system in our body. In the first case (Figure 5a), there is an increase in the temperature by $2K$, $18K$, and $45K$ for the incident power of 10mW, 100mW, and 250mW, respectively. The temperature rise is pretty high for 100mW and 250mW and could lead to irreversible damage. In the second case, i.e., the THz beam case, the rise is not as high as NIR, mainly due to the incident power. There is a rise of $0.5K$, $1.5K$, and $7K$ for the incident power of 0.5mW, 1mW, and 5mW. We chose such a range of powers due to the scarcity of high power THz sources. Here, a 10mW NIR beam leads to a $2K$ temperature rise, while a 5mW THz beam leads to a rise of $7K$. This notable change is due to the high absorption coefficient in the THz range.

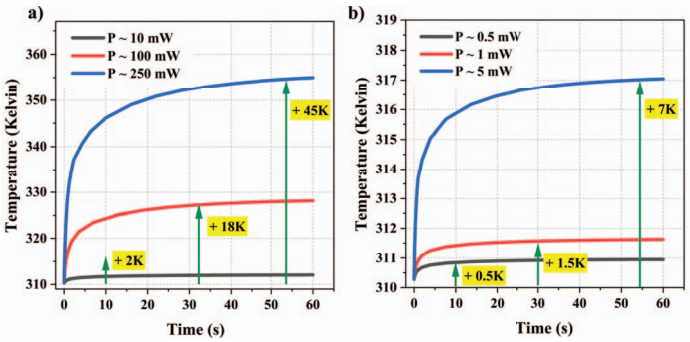

Fig. 5. (a) Temperature rise observed by varying the NIR power source such as 10mW, 100mW and 250mW, (b) Temperature rise observed by varying the THz power source such as 0.5mW, 1mW and 5mW.

In this subsection, we study the effects of varying beam waist by keeping the power constant. Here, we chose a power of 100mW for the NIR case and 1mW for the THz case. The beam waist plays a vital role in controlling the temperature rise. We chose three beam waists - 0.1mm, 0.5mm, and 1mm. The temperature rise follows a similar asymptotic trend as before. The smaller the beam size, the larger the rise in temperature. Decreasing the beam size increases the power

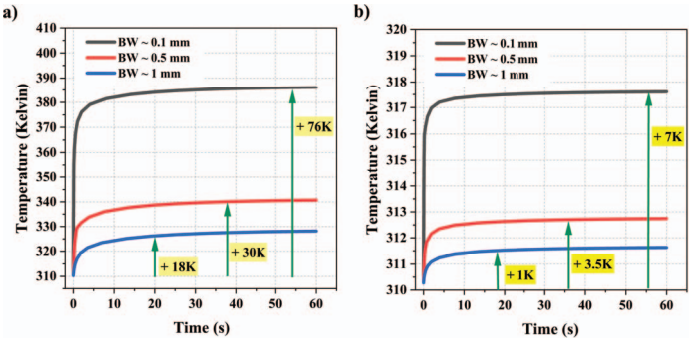

Fig. 6. (a) Temperature rise observed by varying the beam waist of NIR power source from 0.1mm to 1mm. (b) Temperature rise observed by varying the beam waist of THz power source from 0.1mm to 1mm.

density, and thereby increases the temperature. Interestingly, the rise in temperature does not scale linearly with the rate at which beam size reduces. It might be due to the quadratic relation between power density and the beam waist. Overall, the beam waist is one of the crucial parameters that can be used to control the photothermal effects.

F. Pulsed mode

The analysis performed in the previous sections assumes a continuous wave source. To control the temperature rise, one can also use time as a variable. Turning on and turning off the source periodically provides the tissue time to dissipate energy and reduce the overall temperature. These types of sources are referred to as Pulsed sources and are often used in medical applications. Pulsed sources fulfill the idea of using the high-power EM wave as a medium of communication by bringing control over the photothermal effects. We use the duty cycle of the pulse as a parameter to control the temperature rise. As we can notice in Figure 7a, when the pulse is ON, there is a gradual rise in the temperature. When the pulse is OFF, there is a substantial drop in the temperature. The dotted line represents the time pulse, and the amount of time it is ON defines the duty cycle. This process occurs periodically every second. Higher the duty cycle, the higher the rise in temperature and vice-versa. In Figure 7b, we plotted the variation in temperature observed with a continuous source vs pulsed source to get a clear understanding. We chose a NIR wavelength of 1200nm, with a power of 250mW in this case. The continuous source keeps increasing the temperature and saturates, leading to an overall temperature rise of 45K. Now, the same source is multiplied by a pulse with varying duty cycles. It mimics the behavior of a pulsed source. When the duty cycle is about 40%, i.e., when the pulse is on for 0.4sec in every 1sec interval, the temperature fluctuates along with the applied pulse. The overall behavior/trend is similar to a continuous source but has an overall temperature rise of 16K. There is a drop of 29K in this case. When the duty cycle is varied to 10%, the temperature saturates to 315K, a mere 4.5K increase in the temperature. For a 10% duty cycle, the temperature rise is equivalent to 10% of the rise in the continuous wave scenario. This analytical approximation helps us determine the duty cycle based on the continuous source temperature rise. Usually, a high-temperature rise is observed in the superficial layers of skin as the light intensity is also high in this region.

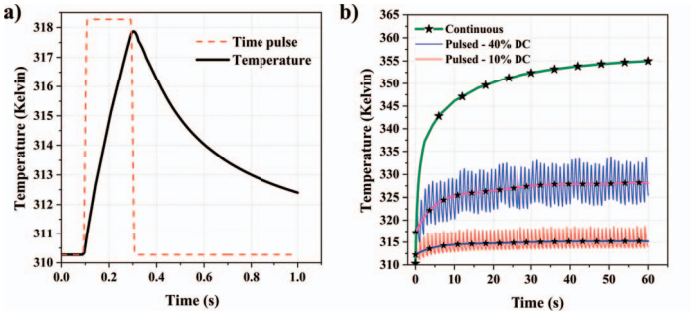

Fig. 7. (a) A 0.2 second time pulse along with the temperature variation, (b) A comparison of continuous and pulsed source induced temperature variation.

IV. Conclusion

We have developed a fully coupled parametric model that estimates the EM wave intensity distribution in human tissue and the subsequent photothermal effects. The model uses diffusion approximation of the radiative transfer equation to predict the intensity variation along the layers of skin. We compared the diffusion approximation with analytical and the Monte Carlo models, using 2D distribution plots and 1D intensity variation plots. We have also showcased the effect of melanin content on the light distribution inside the skin. We then moved to the photothermal analysis to foretell the temperature rise due to the incident wave. We performed the parametric analysis by varying some basic parameters like the power and the beam waist of the source. We illustrated the critical features of these parameters on the temperature rise. Finally, we demonstrated the effect of pulsed sources on the temperature rise and explained how one could use this feature to control the photothermal effects. As part of the future work, we will leverage this model to inform the design of safety limits in future 6G macro- and nano-scale networks.

Acknowledgment

The authors would like to thank Dr. Viktor Sukhotskiy for his suggestions while building the models.

References

[1] M. Seyedi, B. Kibret, D. T. H. Lai, and M. Faulkner, "A survey on intrabody communications for body area network applications," *Ieee Transactions on Biomedical Engineering*, vol. 60, no. 8, pp. 2067–2079, 2013.

[2] D. Naranjo-Hernandez, A. Callejon-Leblic, Z. L. Vasic, M. Seyedi, and Y. M. Gao, "Past results, present trends, and future challenges in intra-body communication," *Wireless Communications & Mobile Computing*, 2018.

[3] J. Heikenfeld, A. Jajack, J. Rogers, P. Gutruf, L. Tian, T. Pan, R. Li, M. Khine, J. Kim, J. Wang, and J. Kim, "Wearable sensors: modalities, challenges, and prospects," *Lab on a Chip*, vol. 18, no. 2, pp. 217–248, 2018.

[4] J. Andreu-Perez, D. R. Leff, H. M. D. Ip, and G. Z. Yang, "From wearable sensors to smart implants-toward pervasive and personalized healthcare," *Ieee Transactions on Biomedical Engineering*, vol. 62, no. 12, pp. 2750–2762, 2015.

[5] M. Pierobon and I. F. Akyildiz, "A physical end-to-end model for molecular communication in nanonetworks," *IEEE Journal on Selected Areas in Communications*, vol. 28, no. 4, pp. 602–611, 2010.

[6] L. Galluccio, T. Melodia, S. Palazzo, and G. E. Santagati, "Challenges and implications of using ultrasonic communications in intra-body area networks," in *2012 9th Annual Conference on Wireless On-Demand Network Systems and Services (WONS)*. IEEE, 2012, pp. 182–189.

[7] S. Banou, M. Swaminathan, G. R. Muns, D. Duong, F. Kulsoom, P. Savazzi, A. Vizziello, and K. R. Chowdhury, "Beamforming galvanic coupling signals for iomt implant-to-relay communication," *IEEE Sensors Journal*, vol. 19, no. 19, pp. 8487–8501, 2018.

[8] I. F. Akyildiz and J. M. Jornet, "Electromagnetic wireless nanosensor networks," *Nano Communication Networks*, vol. 1, no. 1, pp. 3–19, 2010.

[9] J. M. Jornet and I. F. Akyildiz, "Information capacity of pulse-based wireless nanosensor networks," in *2011 8th Annual IEEE Communications Society Conference on Sensor, Mesh and Ad Hoc Communications and Networks*, Conference Proceedings, pp. 80–88.

[10] I. F. Akyildiz and J. M. Jornet, "The internet of nano-things," *IEEE Wireless Communications*, vol. 17, no. 6, pp. 58–63, 2010.

[11] I. F. Akyildiz, M. Pierobon, S. Balasubramaniam, and Y. Koucheryavy, "The internet of bio-nano things," *IEEE Communications Magazine*, vol. 53, no. 3, pp. 32–40, 2015.

[12] Y. Gao, Z. Xin, B. Zeng, Q. Gan, X. Cheng, and F. J. Bartoli, "Plasmonic interferometric sensor arrays for high-performance label-free biomolecular detection," *Lab on a Chip*, vol. 13, no. 24, pp. 4755–4764, 2013. [Online]. Available: http://dx.doi.org/10.1039/C3LC50863C

[13] V. V. Tuchin, "Tissue optics and photonics: light-tissue interaction," *Journal of Biomedical Photonics & Engineering*, vol. 1, no. 2, pp. 98–134, 2015.

[14] L. Carroll and T. R. Humphreys, "Laser-tissue interactions," *Clinics in Dermatology*, vol. 24, no. 1, pp. 2–7, 2006.

[15] F. A. Jolesz, A. R. Bleier, P. Jakab, P. W. Ruenzel, K. Huttl, and G. J. Jako, "Mr imaging of laser-tissue interactions," *Radiology*, vol. 168, no. 1, pp. 249–253, 1988.

[16] B. E. Dibernardo, J. Reyes, and B. Chen, "Evaluation of tissue thermal effects from 1064/1320-nm laser-assisted lipolysis and its clinical implications," *Journal of Cosmetic and Laser Therapy*, vol. 11, no. 2, pp. 62–69, 2009.

[17] H. Guo, P. Johari, J. M. Jornet, and Z. Sun, "Intra-body optical channel modeling for in vivo wireless nanosensor networks," *IEEE Transactions on NanoBioscience*, vol. 15, no. 1, pp. 41–52, 2016.

[18] H. Elayan, P. Johari, R. M. Shubair, and J. M. Jornet, "Photothermal modeling and analysis of intrabody terahertz nanoscale communication," *IEEE Transactions on NanoBioscience*, vol. 16, no. 8, pp. 755–763, 2017.

[19] P. Johari and J. M. Jornet, "Nanoscale optical wireless channel model for intra-body communications: Geometrical, time, and frequency domain analyses," *IEEE Transactions on Communications*, vol. 66, no. 4, pp. 1579–1593, 2018.

[20] G. V. G. Baranoski and A. Krishnaswamy, "An introduction to light interaction with human skin," *2004*, vol. 11, no. 1, p. 30, 2004.

[21] Y. Hasegawa, Y. Yamada, M. Tamura, and Y. Nomura, "Monte carlo simulation of light transmission through living tissues," *Applied Optics*, vol. 30, no. 31, pp. 4515–4520, 1991.

[22] G. B. Ma, J. F. Delorme, P. Gallant, and D. A. Boas, "Comparison of simplified monte carlo simulation and diffusion approximation for the fluorescence signal from phantoms with typical mouse tissue optical properties," *Applied Optics*, vol. 46, no. 10, pp. 1686–1692, 2007.

[23] W. F. Cheong, S. A. Prahl, and A. J. Welch, "A review of the optical-properties of biological tissues," *Ieee Journal of Quantum Electronics*, vol. 26, no. 12, pp. 2166–2185, 1990.

[24] A. J. Welch, "The thermal response of laser irradiated tissue," *Ieee Journal of Quantum Electronics*, vol. 20, no. 12, pp. 1471–1481, 1984.

[25] K. Mitra, S. Kumar, A. Vedavarz, and M. K. Moallemi, "Experimental-evidence of hyperbolic heat-conduction in processed meat," *Journal of Heat Transfer-Transactions of the Asme*, vol. 117, no. 3, pp. 568–573, 1995.

[26] J. Liu, X. Chen, and L. X. Xu, "New thermal wave aspects on burn evaluation of skin subjected to instantaneous heating," *Ieee Transactions on Biomedical Engineering*, vol. 46, no. 4, pp. 420–428, 1999.

[27] B. Shen and P. Zhang, "Notable physical anomalies manifested in non-fourier heat conduction under the dual-phase-lag model," *International Journal of Heat and Mass Transfer*, vol. 51, no. 7-8, pp. 1713–1727, 2008.

[28] C. H. Li, J. M. Miao, K. X. Yang, X. S. Guo, J. Tu, P. T. Huang, and D. Zhang, "Fourier and non-fourier bio-heat transfer models to predict ex vivo temperature response to focused ultrasound heating," *Journal of Applied Physics*, vol. 123, no. 17, 2018.

[29] H. H. Pennes, "Analysis of tissue and arterial blood temperatures in the resting human forearm (reprinted from journal of applied physiology, vol 1, pg 93-122, 1948)," *Journal of Applied Physiology*, vol. 85, no. 1, pp. 5–34, 1998.

[30] F. Xu, T. J. Lu, K. A. Seffen, and E. Y. K. Ng, "Mathematical modeling of skin bioheat transfer," *Applied Mechanics Reviews*, vol. 62, no. 5, 2009.

[31] D. E. J. G. J. Dolmans, D. Fukumura, and R. K. Jain, "Photodynamic therapy for cancer," *Nature Reviews Cancer*, vol. 3, no. 5, pp. 380–387, 2003.

[32] X. Huang and M. A. El-Sayed, "Gold nanoparticles: Optical properties and implementations in cancer diagnosis and photothermal therapy," *Journal of Advanced Research*, vol. 1, no. 1, pp. 13–28, 2010.

[33] M. H. Xu and L. H. V. Wang, "Photoacoustic imaging in biomedicine," *Review of Scientific Instruments*, vol. 77, no. 4, 2006.

[34] J. Laufer, D. Delpy, C. Elwell, and P. Beard, "Quantitative spatially resolved measurement of tissue chromophore concentrations using photoacoustic spectroscopy: application to the measurement of blood oxygenation and haemoglobin concentration," *Physics in Medicine and Biology*, vol. 52, no. 1, pp. 141–168, 2007.

[35] D. Huang, E. A. Swanson, C. P. Lin, J. S. Schuman, W. G. Stinson, W. Chang, M. R. Hee, T. Flotte, K. Gregory, C. A. Puliafito, and J. G. Fujimoto, "Optical coherence tomography," *Science*, vol. 254, no. 5035, pp. 1178–1181, 1991.

[36] "Comsol multiphysics ^{TM} v. 5.6. www.comsol.com., comsol ab, stockholm, sweden."

[37] F. Martelli, *Light propagation through biological tissue and other diffusive media : theory, solutions, and software / Fabrizio Martelli [and others]*. Bellingham, Wash: SPIE Press, 2010.

[38] S. L. Jacques, "Optical properties of biological tissues: a review," *Physics in Medicine and Biology*, vol. 58, no. 11, pp. R37–R61, 2013.

[39] L. Wang, S. L. Jacques, and L. Zheng, "Mcml—monte carlo modeling of light transport in multi-layered tissues," *Computer Methods and Programs in Biomedicine*, vol. 47, no. 2, pp. 131–146, 1995.

[40] A. N. Bashkatov, E. A. Genina, V. I. Kochubey, and V. V. Tuchin, "Optical properties of human skin, subcutaneous and mucous tissues in the wavelength range from 400 to 2000 nm," *Journal of Physics D - Applied Physics*, vol. 38, no. 15, pp. 2543–2555, 2005.

[41] G. J. Wilmink, B. L. Ibey, B. D. Rivest, J. E. Grundt, W. P. Roach, T. D. Tongue, B. J. Schulkin, N. Laman, X. G. Peralta, C. C. Roth *et al.*, "Development of a compact terahertz time-domain spectrometer for the measurement of the optical properties of biological tissues," *Journal of biomedical optics*, vol. 16, no. 4, p. 047006, 2011.

[42] E. Pickwell, B. E. Cole, A. J. Fitzgerald, M. Pepper, and V. P. Wallace, "In vivo study of human skin using pulsed terahertz radiation," *Physics in Medicine & Biology*, vol. 49, no. 9, p. 1595, 2004.

[43] S. L. Jacques and D. J. McAuliffe, "The melanosome: Threshold temperature for explosive vaporization and internal absorption coefficient during pulsed laser irradiation," *Photochemistry and Photobiology*, vol. 53, no. 6, pp. 769–775, 1991.